High-sensitivity resonant cavity monitor system with direct RF sampling electronics

Yimei Zhou,[1,*] Longwei Lai,[1,*,†] Jialan Pan,[2,3] Yingbing Yan,[1] Jian Chen,[1] Xiaoqing Liu,[1] Shanshan Cao,[1] Renxian Yuan[1]

[1]Shanghai Advanced Research Institute, Chinese Academy of Sciences, Shanghai 201204, China

[2]Shanghai Institute of Applied Physics, Chinese Academy of Sciences, Shanghai 201800, China

[3]University of Chinese Academy of Sciences, Beijing 100049, China

* These authors contributed to the work equally and should be regarded as co-first authors.

† Corresponding author: lailw@sari.ac.cn

Abstract. Resonant cavity monitors are widely used in Free Electron Lasers (FELs) and proposed for linear collider for high-resolution position and phase measurements. The read-out electronics is a main limiting factor affecting system performance. A prototype cavity monitor system with direct RF sampling electronics was developed for the C-band cavity beam arrival monitors used in SHINE. The diopole-mode frequency of the cavity is 3.52 GHz. The direct RF sampling electronics simplifies the otherwise complex RF front-end applying traditional down-conversion electronics. The direct RF sampling processor use ADCs with -3dB bandwidth of 9 GHz, a maximum sampling rate of 2.6 GSPS, and 8 bits ENOB at 3.52 GHz. A theoretical analysis shows, that the direct-digital down-conversion electronics should have the same performance as an analog RF down-converter, and on-line beam tests at SXFEL verified its high sensitivity. The relative amplitude error of the electronics is 1.3×10^{-4} at 80 pC, and the relative phase error is 8.4 fs. Even with a beam charge of 1 pC, the relative amplitude error of the electronics is better than 1.0×10^{-3}, and the relative phase error is 47.7 fs. It paves the way for large-scale applications of direct RF sampling electronics in SHINE. This represents a significant advancement in beam instrumentation at SHINE, leading to both a reduction in project costs and an enhancement in system reliability.

I. INTRODUCTION

The Shanghai HIgh repetitioN rate XFEL and Extreme light facility (SHINE) is a CW superconducting hard X-ray FEL, the largest scientific project in China to date. SHINE consists of a superconducting LINAC with a beam energy of 8 GeV, three undulator lines delivering photons in the range of 0.4 to 25 keV, three beamlines and ten experimental end-stations. The total length is 3.1 km, the tunnel depth is 29 m underground [1] (Fig.1). SHINE is designed for a maximum bunch repetition rate of 1 MHz, with bunch intensities ranges from 10 pC to 300 pC. As of the time of writing, the installation and commissioning of the injector section have been completed, with the full completion of SHINE scheduled for 2027. To achieve a high lasing efficiency in the undulators, high-resolution monitoring of the beam position, bunch arrival time and intensity are required. Passive, bunched-beam excited cavity resonators are widely used in XFELs due to their high shunt impedance, which allows them to deliver output signals with a high signal-to-noise ratio (SNR). These resonators are commonly applied in beam position monitoring (BPM) and bunch arrival monitoring (BAM) [2,3,4,5,6].

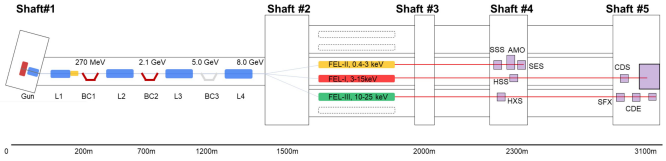

FIG 1. Schematic of the SHINE layout

The dipole-mode frequency of the cavity output signal is primarily determined by the operating frequency of the RF gun, the cutoff frequency of the beam pipe, as well as the geometry and design of the cavity. Most cavity BPMs are operating in the C-band (4 GHz – 8GHz), S-band (2 GHz – 4 GHz) and X-band (8 GHz – 12GHz), and a very few in the L-band (1 GHz – 2 GHz) and Ku-band (12 GHz – 18 GHz). For example, for the Linac Coherent Light Source(LCLS-I, LCLS-II), a high-Q (Q: quality factor) cavity-BPM (CBPM) was developed operating in the X-band, and achieving a position resolution of 200 nm at a charge of 200 pC [1]. A low-Q C-band CBPM was developed in European X-ray FEL (EXFEL), achieving a positional resolution of 183 nm at a bunch charge of 180 pC and a dynamic range of ±500 μm [2]. The high-Q C-band CBPM developed for the SXFEL expected to achieve a resolution of 177 nm at a bunch charge of 500 pC [2].

Read-out electronics are employed for RF signal processing in cavity monitors. High-sensitivity read-out electronics are essential for achieving improved position resolution when extracting position or time (phase) information from the signals of a passive cavity resonator. However, due to the GHz frequency range of these signals, analog-to-digital converters (ADCs) from previous generations are unable to directly sample these signals with the necessary resolution. Figure 2 illustrates the schematic layouts of three different RF signal processing electronics. Traditional methods implement a direct analog I/Q-demodulation (Fig. 2(a)) or utilize the heterodyne principle, a down-conversion of the cavity BPM

RF signals to an intermediate frequency (IF), followed by a digital acquisition and demodulation (Fig. 2(b)). At the SACLA XFEL [5], European-XFEL [9], and Swiss FEL [11] the cavity BPM RF signals are down-converted directly to the I/Q baseband like Fig. 2(a). This technique has the lowest requirements for ADCs and FPGAs, but faces the challenges of analog I/Q imbalance, local oscillator (LO) leakage, low-frequency noise interference, and twice the number of ADCs. At ATF [2], LCLS I/II [7,8], SXFEL [10] and many other FELs the cavity BPM signals are down-converted to an IF like Fig. 2(b), typically in the tens of MHz region, and then digitized at a sufficient high sampling rate to stay in the 1st Nyquist pass-band, typically 100-250 MSPS (Mega Samples Per Second). This structure reduces the difficulties of analog signal processing, and high gain can be obtained by distributing the amplifier at different frequencies. Both structures contain a long and complex analog signal processing chain, and use complex local oscillator synthesizers, mixers, and multistage filters. Image rejection and local oscillator isolation need to be considered, moreover, analog RF components introduce noise and are sensitive to environment changes. Fig. 2(c) illustrates the direct RF sampling electronics, which digitize the RF signal directly using an ADC and subsequently demodulate it through digital signal processing (DSP). Digital signal processing offers several advantages over analog processing. It is programmable and, therefore, flexible, enabling the implementation of perfectly reproducible filters and algorithms for deterministic processing of cavity RF signals, free from issues related to aging, tolerance, and environmental effects [12]. As of the time of writing, ADCs capable of direct RF sampling have sampling rates exceeding 2 GSPS, with analog bandwidths up to 10 GHz, and are commercially available in 12- or 14-bit resolution. This technological advancement makes it an opportune time to develop direct RF sampling monitors for SHINE.

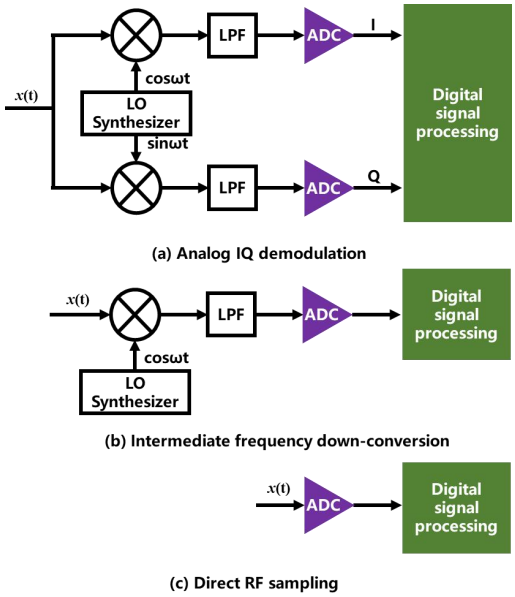

FIG 2. Three types of cavity signal processing electronics

Before writing this paper, the feasibility of using direct RF sampling electronics for C-band cavity probe signal processing was experimentally verified in the laboratory. This validation was carried out using an RF signal generator, a direct RF sampling processor, and an amplification module designed specifically for the experiment [13]. Based on these findings, the design of a cavity BPM/BAM system for SHINE incorporating direct RF sampling electronics was presented in this paper. The paper covers the design of the cavity BPM/BAM, the direct RF sampling electronics, and the associated signal processing algorithms. The performance of the electronics is analyzed in detail and compared with that of the traditional IF down-conversion structure. Additionally, online beam tests are conducted at the SXFEL to evaluate the system's performance in a real-world setting.

II. DESIGN OF CAVITY MONITORS FOR SHINE

Three types of cavity monitors are foreseen for SHINE: cavity BPMs for the distribution line, cavity BAMs for the LINAC, and cavity BPMs for the FEL sections. The cavity BPMs for the distribution line are designed with a 35 mm inner-diameter beam-pipe aperture, with a required resolution of 1 μm at 100 pC and a dynamic range of ±1 mm. The cavity BAMs for the LINAC, also utilizing a 35 mm beam-pipe aperture, require a resolution of 20 fs at 100 pC. For the cavity BPMs in the FEL sections, a smaller 8 mm beam-pipe aperture is used, with a required resolution of 200 nm at 100 pC and a dynamic range of ±100 μm [14]. This section presents the operational principles of cavity monitors and discusses the design considerations for the cavity BPM/BAM system at SHINE.

A. Cavity monitor principle

When a charged particle passes through a cylindrical cavity resonator, all eigen-modes with electric fields aligned along or near the beam axis are excited, causing the beam to dissipate

some of its energy into the resonator. These excited modes carry different beam-related information, and their electromagnetic field can be coupled to narrow-band RF signals for beam observation. The TM_{010} monopole mode is proportional solely to the bunch charge, while the TM_{110} dipole-mode is proportional to both the bunch charge and the transverse position of the beam in the resonator.

A cylindrical cavity resonator can serve as a beam charge monitor (BCM) and a beam arrival time monitor (BAM) by extracting the TM_{010}-mode signal. Additionally, it can function as a beam position monitor (BPM) by utilizing the TM_{110}-mode signals for the two polarizations aligned with the horizontal and vertical axes. In a cylindrical cavity BPM system, the TM_{110}-mode is used for position detection, and the TM_{010}-mode serves as a reference signal. The beam position is determined by normalizing the TM_{110}-mode signal from the position cavity to the TM_{010}-mode signal from the reference cavity. Figure 3 illustrates an electromagnetic simulation of the two eigen-modes as a bunched electron beam passes through a cylindrical cavity.

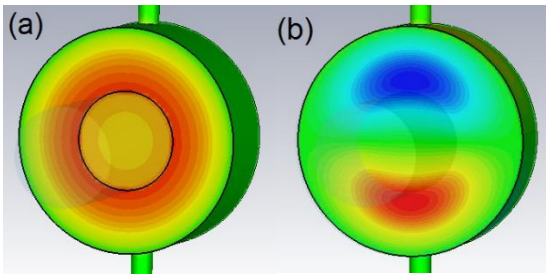

FIG 3. The TM_{010}-mode (a) and TM_{110}-mode(b) in the cylindrical cavity

The voltage signal V_{out} from a cavity probe is modeled as a damped oscillation, described by:

$$V_{out} = A_{RF}\, e^{-t/2\tau} \sin(\omega_{res} t + \phi) \quad (1)$$

Where A_{RF} is the signal amplitude; $\omega_{res} = 2\pi f_{res}$, f_{res} is the resonant frequency of the excited eigen-mode; ϕ is the phase of the signal; τ is the decay time, related to the quality factor of the cavity.

The amplitude of the output signal A_{RF} depends on several factors, including the beam charge q, the geometry of the cavity, and the bunch length σ_z, and is given by [15]:

$$A_{RF} = \frac{\omega_{res}\, q}{2}\sqrt{Q_{ext}\frac{Z}{Q}}\, exp\left(-\frac{\omega_{res}^2 \sigma_z^2}{2c^2}\right) \quad (2)$$

where Z is the characteristic impedance of the cavity; Q_{ext} is the external quality factor, describing the energy coupling to the readout port (P_{out}); c is the speed of light;

$$Q_{ext} = \frac{\omega_{res}\, U}{P_{out}} \quad (3)$$

Where U is the energy stored in the cavity. The energy stored in the cavity also dissipated in the cavity walls. It depends on the wall material and is described by the internal quality factor,

$$Q_0 = \frac{\omega_{res}\, U}{P_{diss}} \quad (4)$$

The energy decay time τ is defined by the loaded quality factor Q_L, which accounts for both external quality factor Q_{ext} and internal quality factor Q_0, can be written as

$$\tau = \frac{Q_L}{\omega_{res}} \quad (5)$$

Where Q_L is given by:

$$\frac{1}{Q_L} = \frac{1}{Q_0} + \frac{1}{Q_{ext}} \quad (6)$$

R/Q (R-over-Q) is the geometric shape factor of the cavity. It is mostly determined by the cavity structure. The R/Q is calculated as:

$$\frac{R}{Q} = \frac{|\int E\, ds|^2}{\omega_{res}\, U} \quad (7)$$

Where E is the electric field along the beam axis, and s is the path along the cavity. The electric field distributions for the TM_{010}-mode and TM_{110}-mode are given by:

$$E_z = C J_0\left(\frac{j_{01} r}{R}\right) e^{-i\omega_{010} t} \quad (8)$$

$$E_z = C J_1\left(\frac{j_{11} r}{R}\right)\cos(\phi) e^{-i\omega t} \quad (9)$$

where C is proportional to the amplitude of the oscillation, J_m is a Bessel function of the first kind of order m, and j_{mn} is the nth root of the equation $J_m(j)=0$. $j_{01}=2.405$, $j_{11}=3.832$. R is the radius of the cavity. The expressions for R/Q for both modes are provided by:

$$\left(\frac{R}{Q}\right)_{110} = \frac{2 J_1^2\left(\frac{j_{11}}{R} x\right) L^2 T^2}{\omega_{110} \varepsilon_0 \pi R^2 J_0^2(j_{11})} \quad (10)$$

$$\left(\frac{R}{Q}\right)_{010} = \frac{2 J_0^2\left(\frac{j_{01}}{R}\right) L^2 T^2}{\omega_{010} \varepsilon_0 \pi R^2 J_1^2(j_{01})} \quad (11)$$

where, x is the beam offset, L is the cavity length, $T = \sin\left(\frac{\omega L}{2c}\right)/\frac{\omega L}{2c}$ is the transit time factor, ε_0 is the vacuum dielectric constant.

B. Design of the cavity BPM and BAM for SHINE

The frequency of SHINE's RF cavities is set at 3.9 GHz. Therefore, the design frequency of the cavity monitors must avoid this value to prevent interference and ensure accurate measurements. Considering the need for a balance between power efficiency, resolution, and manufacturing complexity, the cavity BPM monitors for SHINE are designed to operate in the C-band at frequencies of 3.52 GHz and 5.254 GHz. These frequencies are carefully selected to avoid overlap with the SHINE RF cavity frequency while providing high sensitivity for beam position and arrival time measurements. Furthermore, the cavity BPMs are designed with high loaded quality factors (Q_L) to optimize performance, ensuring stable and accurate signal detection. Table I summarizes the parameters for the two types of cavity BPM monitors planned for SHINE. Type 1 is designed for a 35 mm diameter beam pipe, while Type 2 is intended for an 8 mm diameter beam pipe [16]. Both types are designed with a loaded Q_L that results in a decay time of 200 ns, allowing the system to operate at a bunch repetition rate of 1 MHz without aliasing, thus ensuring reliable beam diagnostics over extended periods of operation.

TABLE I. Parameters of cavity BPMs in the SHINE.

Cavity type	Type 1		Type 2	
Parameters	Position	Reference	Position	Reference
Frequency /GHz	3.520	3.520	5.254	5.254
Radius/mm	51.9	32.6	34.8	21.8
Length/mm	9	4.5	9	5
Decay time /ns	200	200	200	200
Bandwidth /MHz	1.59	1.59	1.59	1.59
Loaded Q	2212	2212	3301	3301
Q_{ext}	3245	5869	5663	1268
Normalized shunt impedance	0.175@ 1mm	50.65	0.56@1 mm	82.6
Sensitivity /V/nC	0.575@ 1mm	7.26	1.15@1 mm	9.4

Figure 4 illustrates the longitudinal cross-section and prototype of the cavity Beam Arrival Monitor (BAM) designed for SHINE. The key dimensions and parameters of the cavity are detailed in Table II. The coupled output signal was measured to be approximately 0.5 V peak at t=0 for a bunch charge of 100 pC.

TABLE II. Design of cavity BAM in the SHINE.

Parameters	Value
Frequency/GHz	3.520
Decay time/ns	200
Bandwidth/MHz	1.59
Q_L	2213
Sensitivity /V/nC	5.2
D_{pipe}/mm	70
R_{gap}/mm	26
L_{cav}/mm	5
L_{gap}/mm	14.8
R_{cav}/mm	30
d_p/mm	1.7

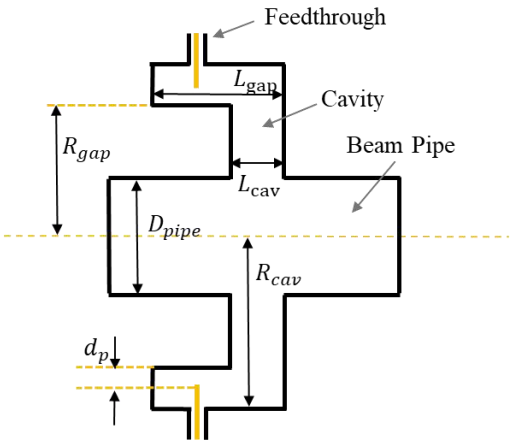

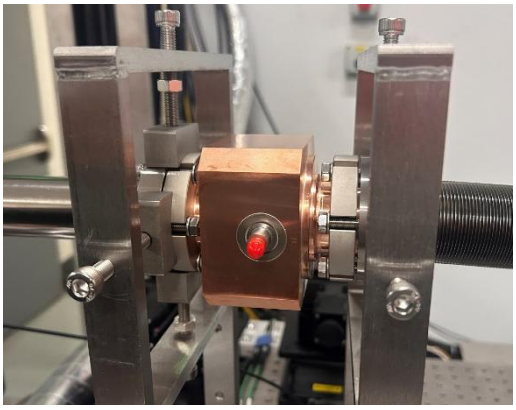

FIG 4. Design and photo of SHINE CBAM.

A cavity BAM prototype for SHINE was fabricated and installed in the SXFEL for an evaluation of the system. The SXFEL operates at a bunch charge of 500 pC. The RF frequency of SXFEL is 2856 MHz, and the synchronized clock is 119 MHz. Fig. 5 shows the sampled raw data and spectrum of the BAM signal using an oscilloscope with 6 GHz bandwidth. The signal spectral component is 3.524 GHz. Another spectral component is observed at 4.36 GHz, which is introduced due to the design of the cavity structure. However, as the noise level of the spectrum is approximately 20 dB below the observed main spectral signal component, and the subsequent signal processing method is only applied to the main spectral component, it has no effect on our measurements.

A prototype of the cavity BAM for SHINE was fabricated and installed in the SXFEL for system evaluation. The SXFEL operates with a bunch charge of 500 pC, an RF frequency of 2856 MHz, and a synchronized clock of 119 MHz. Figure 5 presents the sampled raw data and spectrum of the BAM signal, acquired using an oscilloscope with a 6 GHz bandwidth. The main spectral component of the signal is observed at 3.524 GHz, in line with the design specifications of the BAM. An additional spectral component at 4.36 GHz is also observed, which arises due to the cavity structure design. However, since the noise level of this secondary spectral component is approximately 20 dB lower than the main signal component, and subsequent signal processing is applied exclusively to the primary spectral component, this additional spectral component does not affect the accuracy of the measurements.

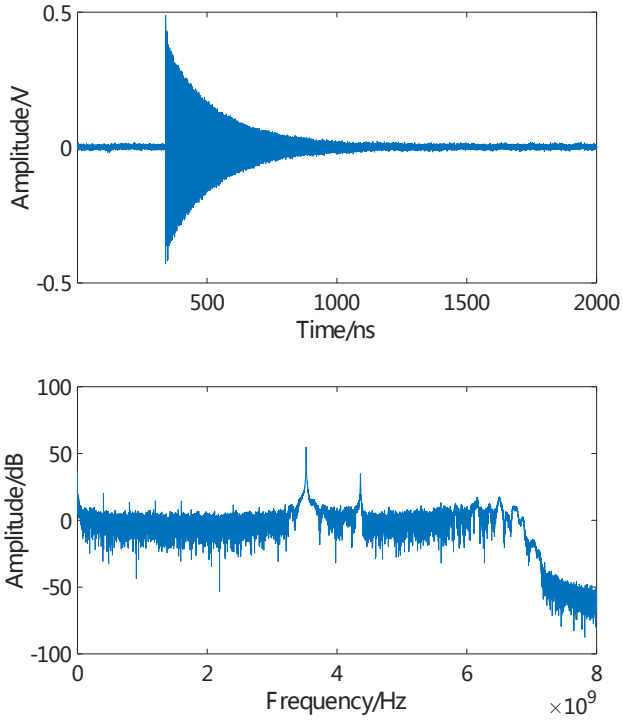

FIG 5. Output signal of cavity BAM.

III. DESIGN OF DIRECT RF SAMPLING ELECTRONICS PROTOTYPE

In contrast to traditional down-conversion electronic, direct RF sampling electronics rely on a significantly reduced number of analog components, resulting in lower noise introduction. This design leads to a higher signal-to-noise ratio (SNR) at the input of the RF direct sampling electronics compared to down-conversion systems. However, as the input signal frequency increases, the SNR of the analog-to-digital converter (ADC) in the direct RF sampling electronics decreases due to clock jitter [17]. As a result, the SNR of the direct RF sampling system becomes lower than that of the down-conversion electronics at higher frequencies. Understanding the magnitude of this SNR reduction is essential for assessing the performance of the electronics.

In this section, we present the design of a direct RF sampling electronics prototype for the SHINE cavity BPM/BAM systems. For comparison, traditional down-conversion electronics were also developed. Performance analyses, as well as online beam tests, have been conducted to evaluate and compare the performance of both electronic systems. These evaluations provide important insights into the advantages and limitations of the direct RF sampling approach for SHINE's beam monitoring applications.

A. Direct RF sampling prototype electronics.

The cavity monitor prototype electronics consist of two main components: a direct RF sampling processor and a signal amplifier module.

1. Direct RF sampling processor

A direct RF sampling processor has been developed

leveraging state-of-the-art electronics technologies, including RF direct sampling analog-to-digital converters (ADCs), high-performance system-on-chip (SoC) field-programmable gate arrays (FPGAs), and low-jitter phase-locked-loop (PLL) oscillators for clock signal generation. The processor is housed as a standalone unit within a 1U high, 19-inch enclosure. The system architecture comprises an FPGA carrier board, two FPGA Mezzanine Card (FMC) connector slots—one for an ADC board and the other for a timing board based on the White Rabbit (WR) standard [18]. The WR timing system ensures precise synchronization of the processor with other components in the SHINE system, facilitating accurate beam measurements and real-time data acquisition. This compact and modular design provides ease of integration into the overall beam monitoring infrastructure while maintaining high performance and reliability.

The ADC board is primarily composed of two ADC chips and PLL circuits. Each ADC features a bandwidth of 9 GHz, a maximum sampling rate of 2.6 GSPS, and a quantization resolution of 14 bits. The effective number of bits (ENOB) of the ADC is approximately 9 bits at an input frequency of 3.52 GHz and 8 bits at 5.25 GHz. The ADC chips utilize a dual converter architecture with JESD204B-encoded serial digital outputs, employing 8 high-speed JESD204B lanes, each capable of achieving a data rate of up to 16 Gbps. Compared to CMOS and LVDS, the JESD204B serial data interface reduces the number of pins, minimizing package size and conductor track complexity, which simplifies board design and reduces overall system costs. This makes JESD204B a widely adopted solution in direct RF sampling ADC chips [19].

The sampling clock is synchronized to the external clock of the electron gun photocathode laser using a two-stage PLL system. This system consists of the LMX2582 PLL synthesizer and the LMK04832 clock jitter cleaner, both from Texas Instruments. The PLL system ensures synchronization of the sampling frequency over a broad range. For SHINE, the RF frequency is 1.3 GHz, and the external synchronized clock is set to 1.3/6 GHz, corresponding to 216.667 MHz. The ADC sampling clock can be synthesized to a frequency of up to 2.6 GHz. For the SXFEL, with an RF frequency of 2.856 GHz, the external synchronized clock is 2.856/24 GHz, or 119 MHz, enabling the ADC sampling clock to be synthesized to 1.904 GHz.

The carrier board for the direct RF sampling electronics is built around the Xilinx FPGA UltraScale+ multi-processor system-on-chip (MPSoC) XCZU15EG. This chip integrates a 64-bit quad-core Arm® Cortex®-A53 processor, a dual-core Arm® Cortex-R5F processor, and Xilinx programmable logic (PL) into a single device. Additionally, it includes on-chip memory, external multiport memory interfaces, and an extensive range of peripheral connectivity options [20]. The FPGA features 24 gigabit transceiver high-speed (GTH) lanes, capable of supporting data rates up to 12.5 Gbps, which are used for transmitting ADC data via the JESD204B protocol. Each ADC is supported by 8 GTH lanes.

The integration of the processing system (PS) and programmable logic (PL) into a single chip significantly simplifies the design of the digital board. The carrier board further incorporates four small form-factor pluggable (SFP) ports, dual data rate (DDR) memory for both PS and PL, interlock outputs, a user input/output system (IOS), a secure digital (SD) card slot, and a joint test action group (JTAG) interface. Figure 6 illustrates both the block diagram and the physical layout of the processor.

The processor is also equipped with an FMC low-pin-count (LPC) slot, which interfaces with the SHINE WR card, allowing the processor to receive a 1.003086 MHz trigger signal and bunch ID from the card for accurate data processing and synchronization. This setup ensures robust synchronization for the system's operation and efficient handling of data.

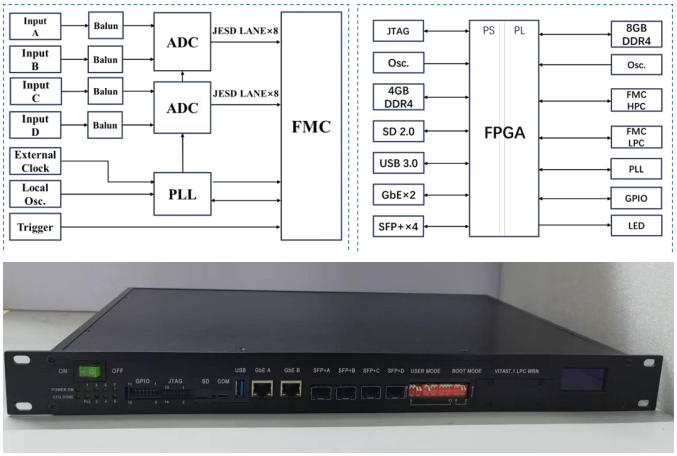

FIG 6. Direct RF sampling processor.

2. RF signal amplifier

The primary advantage of direct RF sampling electronics is the elimination of the need for analog down-conversion, streamlining the overall system architecture. However, a gain/attenuation stage is still essential to ensure that the input signal to the ADC is at an optimal level for accurate sampling. To address this requirement, an independent RF signal amplifier prototype was developed, consisting of four channels housed within a single module. Figure 7 illustrates the structure of one channel, along with a photo of the prototype.

Each RF amplifier channel consists of a low-noise amplifier (LNA) PMA3-63GLN+, which provides a gain of up to 27.9 dB at 3.5 GHz, a high-pass filter HFCN-2700, and a digital-step attenuator RFSA3715 with an attenuation range of

0 to31.75 dB. While the high-pass filter is included in the prototype design, it is not strictly necessary for practical operation. The LNA amplifies the RF signal with minimal noise contribution, ensuring that the signal is conditioned for optimal ADC input. The digital-step attenuator provides fine control over the signal amplitude, facilitating precise adjustments to maintain the required signal levels for ADC processing. This RF amplifier module plays a crucial role in conditioning the RF signal, ensuring that the direct RF sampling electronics perform optimally within the SHINE cavity BPM/BAM system.

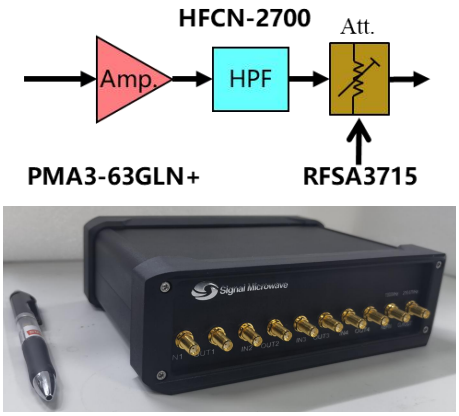

FIG 7. RF signal amplifier prototype.

B. RF down-conversion electronics for comparison

In parallel with the development of the direct RF sampling processor, a set of traditional down-conversion electronics was also developed to enable a performance comparison at the SXFEL. This system comprises an RF down-conversion module and a generic 1 GSPS beam signal processor for SHINE. The RF down-conversion module includes a clock divider and multiplier circuits to generate a local oscillator (LO) signal at 3.466 GHz from the 2856 MHz input signal. It then down-converts the 3.52 GHz input signal to 54 MHz using a mixer and a low-pass filter. Additionally, the module incorporates band-pass filters, low-noise bypass amplifiers, and step attenuators to optimize signal quality.

Figure 8 shows both the block diagram and a photograph of the front-end module and the generic processor. When compared to the direct RF sampling verification module (as shown in Figure 7), the down-conversion front-end module is considerably more complex and larger.

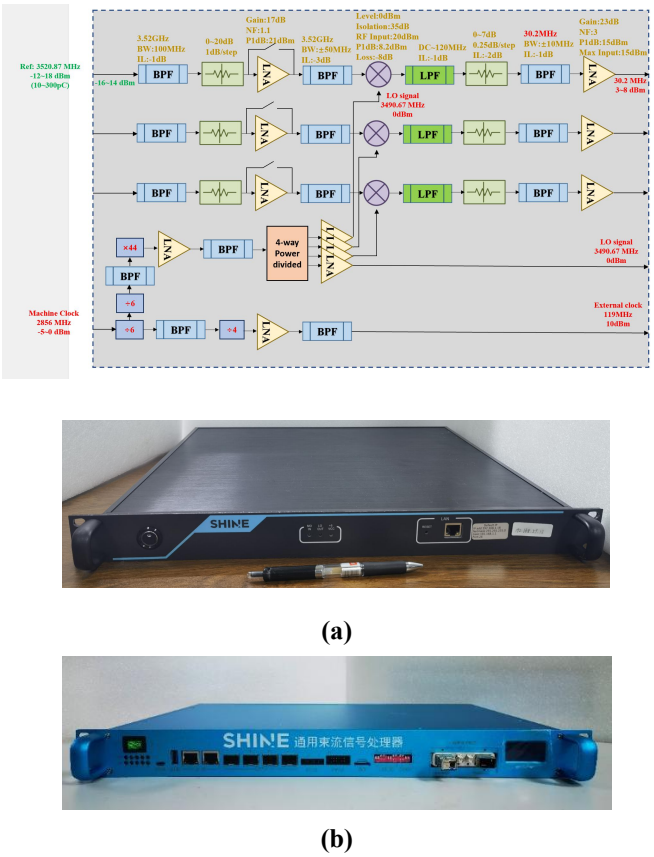

(a)

(b)

FIG 8. Block diagram and picture of RF down-conversion module(a) and the generic processor for SHINE(c).

The generic beam diagnostic processor for SHINE was developed with a design largely similar to the direct RF sampling processor. It utilizes the same carrier board as the direct RF sampling processor, but with modifications to the ADC board. The ADC board is equipped with four-channel ADCs, offering a 2 GHz bandwidth, a maximum sampling rate of 1.0 GSPS, and 14-bit quantization [14]. For operation in the SXFEL, the sampling rate can be configured to 952 MSPS, enabling optimal signal acquisition and processing for the beam diagnostics at the facility.

C. Electronics performance analysis.

The performance of the electronics is mainly determined by analog components and ADC.

1. Analog components performance

The noise figure (NF) is a key parameter used to assess the degradation in signal-to-noise ratio (SNR) as a signal passes through an electronic component or system. It is defined as the ratio of the signal-to-noise ratio at the input to the signal-to-noise ratio at the output, typically expressed in decibels (dB). The noise figure quantifies how much noise is added by the device relative to an ideal noiseless system [21]. Mathematically, the noise figure is expressed as:

$$NF = 10 * log_{10}(F) \quad (12)$$

where F is the noise factor $F = \frac{S_i / N_i}{S_o / N_o}$, S_i/S_o is the

power of input/output signals of the gain stage, N_i/N_o is the power of input/output noise of the gain stage.

The NF of cascaded gain stages *Gn* is calculated as follows:

$$\begin{aligned} F &= F_1 + \frac{F_2 - 1}{G_1} \\ &+ \frac{F_3 - 1}{G_1 * G_2} \\ &+ \frac{F_4 - 1}{G_1 * G_2 * G_3} + \cdots \end{aligned} \tag{13}$$

Where *Fn* and *Gn* are the noise factor and the gain of the nth gain stage. The NF of the used RF amplifier PMA3-63GLN+ at 3.5 GHz is 0.7 dB, the gain is 27.9 dB. For passive components, such as the high-pass-filter (HFCN-2700) and the attenuator, the NF is equivalent to the insertion loss. The insertion loss of the used high-pass filter HFCN-2700 is about 0.9 dB at 3.52 GHz, resulting in a NF of 0.9dB and a gain of -0.9 dB. The attenuator RFSA3715 has an insertion loss of about 2.2 dB at 3.52 GHz, with a NF of 2.2 dB and a gain of -2.2 dB when the attenuator is set to 0 dB. Then, the total NF of the RF signal amplifier module is 0.71 dB with a gain of 24.8 dB.

In comparison, the noise figure (NF) of the down-conversion RF module was calculated to be 7.0 dB, with a gain of 22.0 dB. As a result, the NF of the analog section of the direct RF sampling electronics is 6.3 dB lower than that of the down-conversion electronics, indicating a significant improvement in noise performance for the direct sampling approach.

The noise figure (NF) and gain were measured using Keysight's FieldFox microwave analyzer (N9918B) at a frequency of 3.52 GHz. For the prototype amplitude adjustment module of the direct RF sampling electronics, the NF was measured to be 2 dB, with a gain of 21 dB. In contrast, the down-conversion RF module exhibited a NF of 7.5 dB and a gain of 22.7 dB. Consequently, the NF of the analog section of the direct RF sampling electronics is 5.5 dB lower than that of the down-conversion electronics, demonstrating a significant improvement in noise performance.

2. ADC performance

The noise figure of an ADC is calculated as follows [22]:

$$\begin{aligned} NF &= P_{FS\ (dBm)} \\ &+ 174 dBm \\ &- SNR_{ADC} \\ &- 10log_{10}(f_S/2) \end{aligned} \tag{14}$$

where $P_{FS\ (dBm)}$ is the full-scale power in dBm. The $P_{FS\ (dBm)}$ of both the direct RF sampling ADC processor and the 1 GSPS generic processor is identical. The SNR_{ADC} of the direct RF sampling ADC is approximately 58 dB at an input frequency of 3.52 GHz, while the 1 GSPS generic processor is approximately 67 dB at an input frequency of 54 MHz. Given that the sampling rate f_s of the direct RF sampling ADC is twice that of the 1GSPS ADC in SXFEL, the overall NF of the direct RF sampling ADC is 6 dB worse than the 1 GSPS ADC.

In comparison, the overall NF of the direct RF sampling electronics is nearly identical to that of the RF down-conversion electronics. Theoretically, both electronics should offer equivalent performance when processing the signal from the cavity pickup.

D. Digital signal processing in FPGA.

In the FPGA-based signal processing system, digital data from the ADCs is used to extract the amplitude and phase information of the cavity signal. Given the narrow bandwidth of the cavity signal, several algorithms can be employed, such as digital down-conversion (DDC), Hilbert transform, and discrete Fourier transform (DFT). After considering factors such as processing rate, resource utilization, and overall performance, the fixed-point Goertzel-DFT algorithm was selected for this application [13]. The Goertzel-DFT algorithm is well-suited for applications where the signal frequency is predetermined and stable, as is the case in cavity monitoring systems. This algorithm enables efficient computation of the DFT at a specific frequency, minimizing computational complexity and optimizing FPGA resource usage.

$$X(k) = \sum_{n=0}^{N-1} x(n)\, e^{-j\left(\frac{2\pi}{N}\right)kn} \tag{15}$$

Where $x(n)$ is the digitized signal, *N* is the number of sampled points, and *K* is the extracted frequency. The results are complex values $X(k) = I(k) + j \bullet Q(k)$. *I(k)* and *Q(k)* are called the in-phase and quadrature phase components. Then, the signal amplitude *V* and phase φ can be extracted

using the following formula.

$$V(k) = \sqrt{I(k)^2 + Q(k)^2} \quad (16)$$

$$\varphi(k) = \arctan\left(\frac{I(k)}{Q(k)}\right) \quad (17)$$

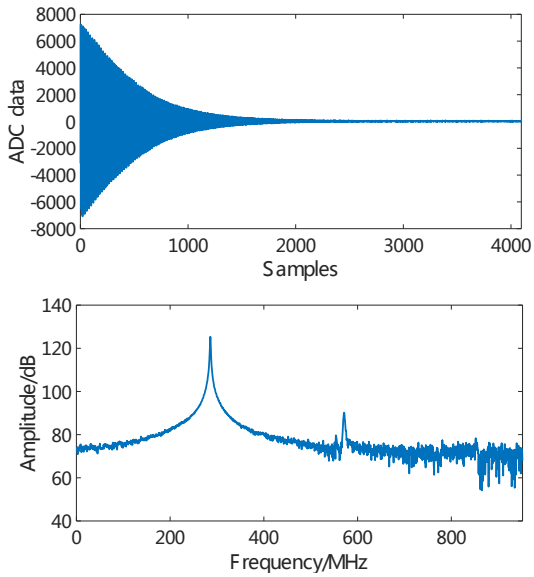

FIG 9. ADC data waveform (a) and spectrum (b) from direct RF sampling

Figure 9 illustrates the data waveform and spectrum of the sampled data obtained from the SHINE BAM prototype installed in the SXFEL. A total of 4096 points are sampled for each beam pulse. It is important to note that due to under-sampling, the center frequency of the cavity signal is shifted and converted to 285.9 MHz.

The relative amplitude error between two channels of electronics can be calculated using the following formula:

$$R_v = std\left(\frac{V1 - V2}{(V1 + V2)/2}\right)/\sqrt{2} \quad (18)$$

where *V1* and *V2* are the amplitude values calculated from the sampled data of the two channels.

The phase error of the electronics is defined as the standard deviation of the phase difference between the two channels:

$$R_p = std(\varphi_1 - \varphi_2)/\sqrt{2} \quad (19)$$

where φ_1 and φ_2 are the phase values calculated from the sampled data of the two channels.

The design bandwidth of the cavity signal is approximately 1.6 MHz. In the DFT algorithm, two methods can be used to obtain the peak amplitude of the cavity signal. First, the fixed-point DFT is calculated using all 4096 samples, where the frequency resolution of each point in the spectrum is 0.47 MHz. Then a summation of points around the center frequency is performed to achieve a reasonable result. Fig. 10(a) illustrates the amplitude obtained from the 4096-point DFT calculation, where sample 615 represents the peak value in the spectrum. Fig. 10(b) displays the relative amplitude error as a function of the number of points accumulated around the peak point. The optimal result, with an error of 1.7×10^{-4}, is achieved when 7 points are summed. Fig. 10(c) shows the phase error, with the peak point exhibiting the best phase accuracy, resulting in a phase error of 14.9 fs. No further improvement in phase error was observed by including additional sample points in the phase calculation.

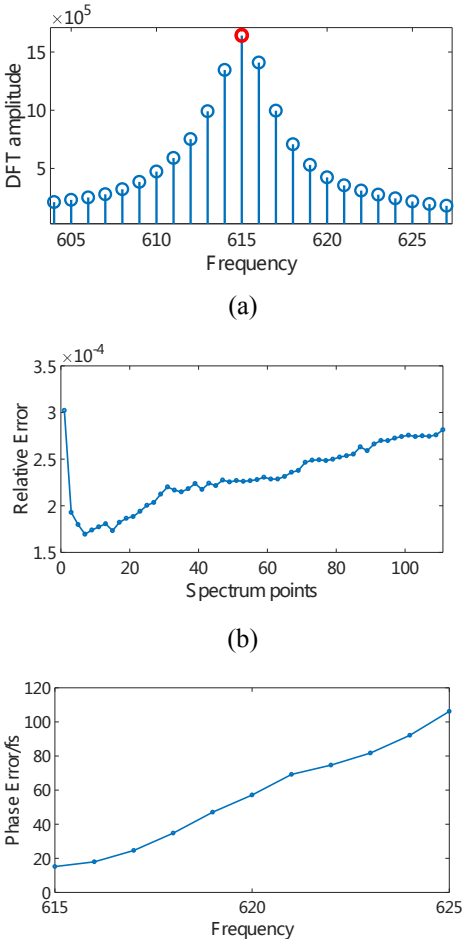

FIG 10. DFT amplitudes around peak point (a), the relative amplitude error of different DFT accumulation points around the peak point (b), and phase error at different DFT point (c).

The second method is to select a subset of data from the start point to calculate the DFT of its center frequency. Fig. 11 shows the performance changes with different DFT length. The best value 1.7×10^{-4} from 500 to 900 points. This is equal to the first method. The phase error is 10.5 fs, which is a little bit better compared to the phase error using the first method.

The second method involves selecting a subset of data from the start point and calculating the DFT for its center frequency.

Figure 11 demonstrates the performance variation with different DFT lengths. The best relative amplitude error, 1.7×10^{-4}, is achieved when using between 500 and 900 points, which is equivalent to the result from the first method. The phase error is 10.5 fs, which is a little bit better compared to the phase error using the first method.

The second method calculates fewer DFT points while achieving better performance. Obviously the second method is better than the first.

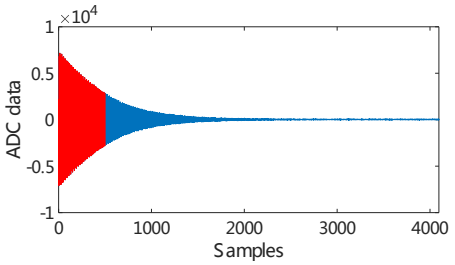

(a)

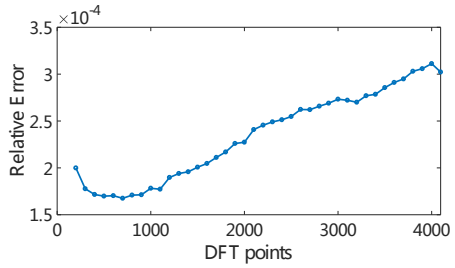

(b)

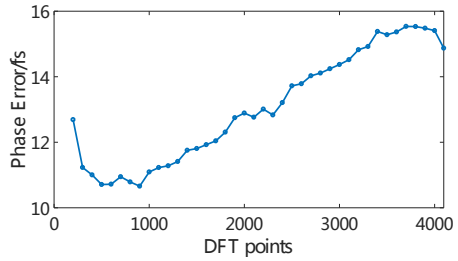

(c)

FIG 11. The subset of sampled data (a), the relative amplitude error (b) and phase error (c) of peak point DFT when computing different data lengths (b).

IV. BEAM TESTS AT THE SXFEL

The manufacturing of a prototype cavity BAM, foreseen for SHINE, was completed and installed at the end of the LINAC section of the SXFEL for online beam experiments, and to evaluate system performance. For our beam tests the SXFEL operated with bunch intensities at approximately 500pC. The output signal of the cavity BAM was transmitted from the tunnel to the cabinet via an approximately 40 meter long, 3/8 inch low-loss coaxial cable type, HELIAX LDF2-50. At the operating frequency of 3.52 GHz, the signal attenuation for the long cables is approximately 10 dB [23]. A four-channel power divider was used to splits the signal, so the input signal to the electronics is equivalent of a bunch intensity of 80 pC.

A. Is a RF band-pass filter (BPF) required?

Band-pass filters are essential in RF analog heterodyne receivers, serving primarily to reject image frequency mixing products, unwanted spurious sidebands, and acting as selective filters for the desired frequency range. It is customary to posit a BPF in front of the direct RF sampling electronics. However, the cavity resonator itself has a band-pass filter characteristic of narrow-band, acting as an effective BPF. Furthermore, unlike down-conversion electronics, RF direct sampling electronics do not generate spurious signals. This is due to the direct sampling approach, where no mixing processes contribute to spurious frequencies. Additionally, the digital signal processing algorithm used in these systems extracts the signal at a fixed-point frequency, further ensuring the isolation of the desired signal. Consequently, it may be possible to eliminate the BPF in direct RF sampling electronics for cavity monitor systems.

Fig. 12(a) illustrates the test setup, where two 3.52 GHz cavity BPFs are connected in front of channels 1 and 2, while channels 3 and 4 are configured without BPFs. The relative amplitude error between channels 1 and 2 (with BPF) is found to be 2.25×10^{-4}, whereas for channels 3 and 4 (without BPF), it is 1.29×10^{-4}, as shown in Fig. 12(b). The phase RMS error is 12.6 fs for channels 1 and 2 (with BPF) and 9.0 fs for channels 3 and 4 (without BPF), as depicted in Fig. 12(c). These results indicate that the inclusion of the BPF does not lead to any improvement in system performance of the SHINE cavity monitor; in fact, it slightly reduces it. Therefore, a BPF is not necessary in the configuration of the direct RF sampling read-out electronics for our system.

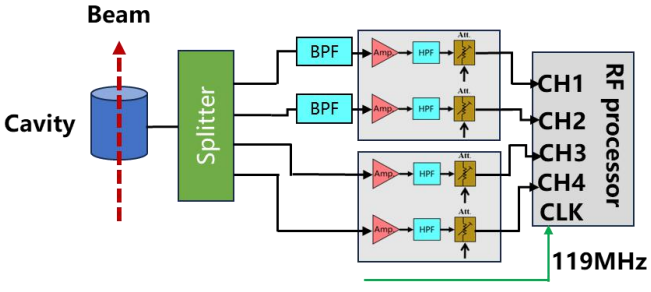

(a)

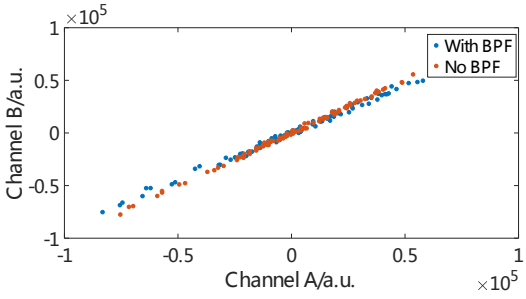

(b)

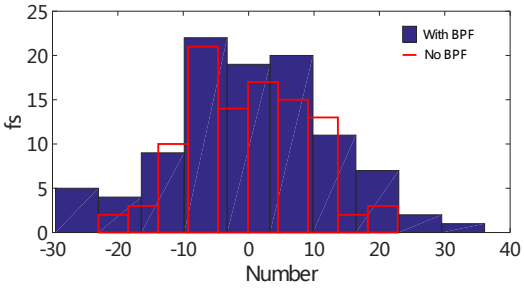

(c)

FIG 12. Test to evaluate BPF necessity (a), the relative amplitude error (b) and phase error (c) with and without BPF.

B. RF signal conditioning performance comparison.

In Section III, the NF of the RF signal amplifier in Fig. 7 is better than that of the down-conversion electronics in Fig. 8 (a). Figure 13 illustrates the test setup for the comparing the performance of the two RF read-out electronics. The 4-way split cavity monitor signals are fed in pairs into the two channels of the two RF modules, which are then sampled with the direct RF sampling processor. The relative amplitude error for the direct RF and down-conversion module is 1.67×10^{-4} and 2.63×10^{-4}, respectively, while the phase jitter is 9.6 fs and 11.0 fs, respectively. It is important to note that the SNR of the direct RF sampling ADC is higher when sampling a down-converted 54 MHz IF input signal compared to a direct 3.52 GHz RF input signal. Despite this, the performance of the RF conditioning prototype is still better than that of the down-conversion RF front-end module.

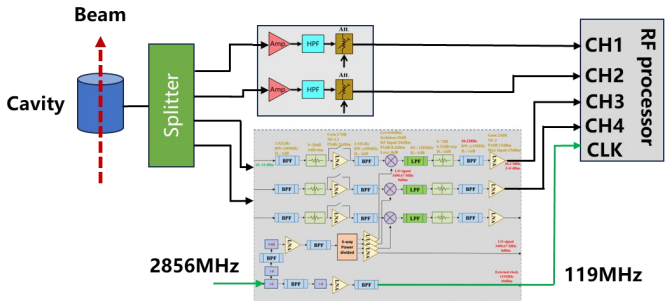

(a)

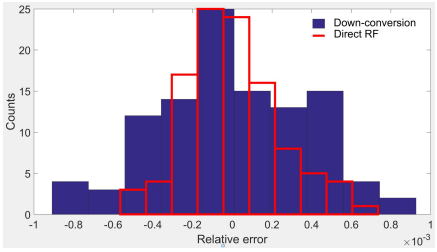

(b)

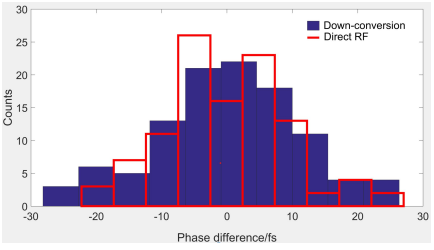

(c)

FIG 13. Test setup to compare RF module performance (a), the relative amplitude error (b) and phase error (c).

C. High-sensitivity performance test.

The charge of the SHINE beam bunches ranges from 10 pC to 300 pC. The electronics designed above are optimized for a bunch charge of 100 pC, but the signal for lower charge is too weak to be detected with a gain of 24.8 dB. Therefore, we cascaded two gain stages of the direct RF sampling module with a cable to double the power gain from 24.8 dB to 49.6 dB while keeping NF almost the same. However, this is not manageable in a simplistic way for the analog RF down-conversion module. Attenuators with different values are added before the power splitter to simulate bunches of different charges. Fig.14 shows the test block diagram.

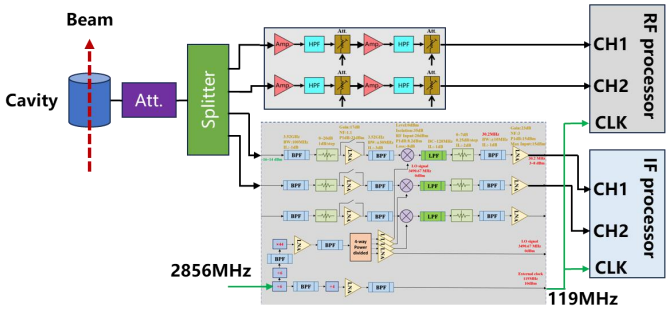

FIG 14. The test of system sensitivity.

Attenuators with different values are connected before the splitter, and the corresponding beam charges are listed in Table 3. The lowest beam charge is 0.8 pC.

TABLE III. The relationship between external attenuator and equivalent beam charge.

External attenuator	Beam charge
0dB	80pC
8dB	32pC
16dB	13pC
20dB	8pC
24dB	5pC
28dB	3pC
34dB	1.6pC
38dB	1pC
40dB	0.8pC

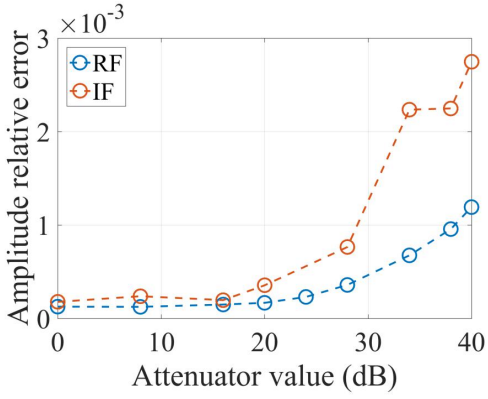

(a)

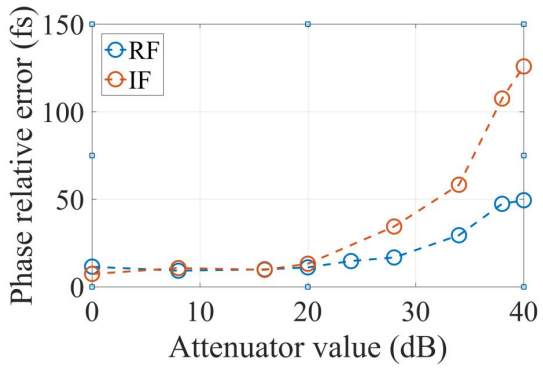

(b)

FIG 15. Relative amplitude error (a) and phase errors (b) with different external attenuators.

Figure 15 shows that the relative amplitude error and phase error of the direct RF and down-conversion modules for different bunch charges. The performance of both modules is similar for bunch charge higher than 8 pC (with a 20 dB attenuator). At 80 pC (0 dB attenuator), the relative amplitude error of the direct RF sampling electronics is 1.3×10^{-4}, while the down-conversion electronics is 1.7×10^{-4}. As the charge continues to decrease, the amplitude and phase errors of direct RF sampling electronics are smaller than those of down-conversion electronics, owing to the higher gain of the direct RF sampling electronics. At a charge of 1 pC, the relative amplitude error is 9.57×10^{-4}, still better than the required 1.0×10^{-3} at SHINE. The charge resolution is 0.96 fC, and the phase resolution is 47.4 fs.

V. CONCLUSIONS

A prototype cavity monitor system with direct RF sampling electronics was developed for SHINE and tested at the SXFEL.

For the beam tests, the cavity monitor foreseen as BAM was used, it operates at a frequency of 3.52 GHz. A theoretical analysis shows, the direct RF sampling electronics has about the same noise performance as the down-conversion electronics. For amplitude and phase extraction, a fixed-point DFT algorithm with a data length of 500 to 900 was found to be the most effective. Online beam tests at SXFEL confirm that a BPF is not required here. The relative amplitude error of the electronics is 1.3×10^{-4} at 80 pC, and the relative phase error is 8.4 fs. At lower charges, such as 1 pC, the relative amplitude error of the electronics still remails below 1.0×10^{-3}, and the phase error is 47.7 fs. These results indicate that the cavity monitoring system with direct RF sampling electronics offers a higher signal sensitivity compared to the traditional analog RF down-conversion technique when RF gain stages are cascaded.

Based on the results of the above tests, a new direct RF sampling electronics for the SHINE cavity BPMs is currently under development. This will represent the first large-scale application of direct RF sampling electronics for cavity monitors operating at C-band. Direct RF sampling electronics play a crucial role in optimizing system structure, enhancing performance, and reducing the cost of beam instrumentation in accelerator.

ACKNOWLEDGEMENTS

This work was supported by the National Science Foundation of China (Grant No.12175293). Youth Innovation Promotion Association, CAS (Grant No. 2019290). Outstanding member of the Youth Innovation Promotion Association, CAS. SHINE R&D and project.

REFERENCE

[1] Zhentang Zhao, H. Ding, B. Liu, Shanghai hard x-ray FEL facility progress status, 15th International Particle Accelerator Conference, Nashville, TN, USA, 2024, p967-972, doi:10.18429/JACoW-IPAC2024-TUZN1

[2] Sean Walston, et al., Performance of a high resolution cavity beam position monitor system, Nucl. Instrum. Methods Phys. Res. 578 (2007) 1–22, DOI:10.1016/j.nima.2007.04.162

[3] Yoichi Inoue, Hitoshi Hayano, Yosuke Honda, et,al. Development of a high-resolution cavity-beam position monitor, Physical Review Special Topics – Accelerators and Beams, 11, 062801 (2008), DOI: 10.1103/PhysRevSTAB.11.062801

[4] Thorsten R. Pusch, F. Frommberger, W. C. A. Hillert, B. Neff, Measuring the intensity and position of a pA electron beam with resonant cavities. Physical Review Special Topics – Accelerators and Beams, 15, 112801 (2012). DOI: 10.1103/PhysRevSTAB.15.112801

[5] H. Maesaka, H. Ego, S. Inoue, S. Matsubara, T. Ohshima, T. Shintake, Y. Otake, Sub-micron resolution rf cavity beam position monitor system at the SACLA XFEL facility, Nuclear Instruments and Methods in Physics Research Section A, Volume 696, 2012,Pages 66-74, DOI : 0.1016/j.nima.2012.08.088.

[6] Chuangye Song, Yanqing Jia, Zhuoyuan Liu, et,al. High-resolution cavity bunch arrival-time monitor
for charges less than 1 pC, Physical Review Accelerators and Beams, 26, 012803 (2023)

[7] Stephen Smith, et al. Commissioning and performance of LCLS cavity BPMs. in Proceedings of PAC09. 2009. Vancouver, BC, Canada.

[8] Josef Frisch, Paul Emma, Alan Fisher, Patrick Krejcik, et al. Electron beam diagnostics and feedback for the LCLS-II. Proceedings of FEL2014, Basel, Switzerland

[9] M. Stadler, et al. Beam test results of undulator cavity BPM electronics for the European XFEL. in Proceedings of IBIC2012. 2012. Tsukuba, Japan.

[10] Chen J, et al. Optimization of the cavity beam-position monitor system for the Shanghai soft X-ray free-electron laser user facility[J]. Nuclear Science and Techniques, 2022, 33(10):1-11.DOI:10.1007/s41365-022-01117-8.
[11] Boris Keil, et al. First beam commission experience with the SwissFEL cavity BPM. Proceedings of IBIC2017, Grand Rapids, MI, USA.
[12] M. Wendt et al., “Direct (Under) sample vs. analog down conversion for BPM electronics”. in Proc. IBIC’14, Monterey, CA, USA, Sep. 2014, Paper MOPAB092 pp. 338-340.
[13] Rong Meng, Longwei Lai, Yimei Zhou, et, al. RF direct sampling and processing electronics for SHINE cavity BPM system, Nuclear Instruments and Methods in Physics Research Section A, Volume 1063, 2024, 169256, DOI: /10.1016/j.nima.2024.169256.
[14] Yuxin Han, Longwei Lai, Yimei Zhou, High performance generic beam diagnostic signal processor for SHINE, in Proceedings of IBIC2024, DOI: 10.18429/JACoW-IBIC2024-WEP53
[15] Nakamura, T., Development of beam-position monitors with high position resolution, in Master’s thesis. 2008, The University of Tokyo.
[16] J. Chen, S.S. Cao, R.X. Yuan, et al., Development and performance evaluation of the CBPM system for the SHINE, the 13th International Beam Instrumentation Conference (IBIC 2024), Beijing, China.
[17] Zaid J. Towfic, Shang-Kee Ting and Ali H. Sayed. Clock jitter compensation in high-rate ADC circuits. IEEE Transactions on signal processing, VOL. 60, NO. 11, NOVEMBER 2012.
[18] Y.B. Yan, P.X.Yu, G.H. Chen, Q.W. Xiao, et, al. White rabbit based beam-synchronous timing systems for SHINE, IPAC2022, Bangkok, Thailand, doi:10.18429/JACoW-IPAC2022-THIYGD1
[19] What Is JESD204 and Why Should We Pay Attention to It?
https://www.analog.com/en/technical-articles/what-is-jesd204-and-why-should-we-pay-attention-to-it.html.
[20] Xilinx, Zynq UltraScale+ MPSoC Data Sheet: Overview. www.xilinx.com
[21]Understanding Noise Figure,https://www.qsl.net/va3iul/Noise/Understanding%20Noise%20Figure.pdf
[22] Walt Kester, ADC Noise Figure—An Often Misunderstood and Misinterpreted Specification https://www.analog.com/media/en/training-seminars/tutorials/MT-006.pdf
[23] LDF2-50 datasheet, https://www.commscope.com/